Applied Catalysis A: General 520 (2016) 24–34

Contents lists available at ScienceDirect

Applied Catalysis A: General

journal homepage: www.elsevier.com/locate/apcata

NiMo catalysts supported on the Nb modified mesoporous SBA-15 and HMS: Effect of thioglycolic acid addition on HDS

Radostina Palcheva[a,*], Luděk Kaluža[b,*], Lubomir Dimitrov[c], Georgi Tyuliev[a], Georgi Avdeev[d], Květa Jirátová[b], Alla Spojakina[a]

[a] Institute of Catalysis, G. Bonchev Str., Bldg. 11, 1113 Sofia, Bulgaria
[b] Institute of Chemical Process Fundamentals, Academy of Sciences of the Czech Republic, Rozvojová 135, 165 02 Prague 6, Czech Republic
[c] Institute of Mineralogy and Crystallography Acad. I. Kostov, Bldg. 107, G. Bonchev Str., 1113 Sofia, Bulgaria
[d] Institute of Physical Chemistry, G. Bonchev, str. Bldg. 11, Sofia, Bulgaria

ARTICLE INFO

Article history:
Received 16 December 2015
Received in revised form 7 April 2016
Accepted 11 April 2016
Available online 12 April 2016

Keywords:
Nb-SBA-15
Nb-HMS
NiMo catalyst
Hds
Complexing agent

ABSTRACT

Nb modified mesoporous SBA-15 and HMS materials were synthesized and studied as a support of NiMo. Calcined co-impregnated NiMo catalysts were prepared using ammonium heptamolybdate and nickel nitrate. Moreover, NiMo catalysts prepared in this manner were treated with thioglycolic acid (TGA). For comparison, NiMo catalysts were prepared by a simultaneous impregnation of the supports with Ni, Mo precursors and TGA. The TGA:Mo molar ratio was 4.0. The supports and NiMo catalysts were characterized by N_2 physisorption, small- and wide-angle XRD, TPD-NH_3, SEM, UV–vis DRS, FTIR and XPS. Catalyst activity was examined in hydrodesulfurization (HDS) reactions of 1-benzothiophene and thiophene at 350 °C. It was found that simultaneous impregnation by Ni, Mo and TGA led to higher HDS activities than the sequential treatment of the calcined NiMo catalysts by TGA.

1. Introduction

Stricter legislative limits on the sulfur content in gasoline lead to higher demands on hydrotreating catalysts. Supported molybdenum sulfide catalysts promoted by Co or Ni have been widely used in industrial HDS processes [1,2]. As proposed by Topsøe et al. [2], the active sites of these catalysts are the so-called Co (Ni)–Mo–S phases, in which Co(Ni) atoms are located on the edges of MoS_2 particles. New active phases different from the conventional Ni–Mo or Co–Mo phases, new supports, as well as new methods of preparation leading to higher concentration of Co(Ni)–Mo–S phase in the catalyst have attracted great interest in the past few years [3,4].

New catalysts containing niobium, unsupported and carbon-supported niobium sulfide, and Ni-doped niobium sulfide catalysts were prepared by the authors [5–7]. Unsupported niobium trisulfide was found to be a better catalyst for the thiophene conversion than molybdenum disulfide. Catalytic activity of the unsupported mixed Ni–Nb sulfide was similar to that observed for Ni–Mo–S [6,7]. For this reason, catalysts containing niobium are interesting to study for the process of hydrodesulfurization (HDS).

Apart from convenient support (alumina), mesoporous silica attracts high attention as support for HDS catalysts because of its high surface area and unique porous structure. In order to tune its chemical and physical properties, the introduction of specific modifiers into the walls of mesostructured silica has received great attention [8–10]. Modification of the mesoporous silica by niobium leads to formation of Nb-containing mesoporous silica with isolated and tetrahedral coordinated Nb-oxide species [11]. In HDS of thiophene, activity of the niobia-supported nickel catalysts was much higher than the activity of the alumina-supported ones. However, the activity of the niobia-supported molybdenum catalysts was lower than that of the alumina-supported catalyst. Concerning NiMo catalysts, low or practically no synergy was observed over niobia-supported catalysts, in sharp contrast to the alumina support [12].

Various methods have been proposed in order to design and prepare highly active Ni (Co)–Mo(W) catalysts. Some of these approaches include the application of organic chelating agents [13–17], novel or modified alumina supports weakly interacting with the active phase [18–24], or novel chemical compounds as precursors, including heteropolycompounds of Keggin type [22,23,25–27]. The use of chelating agents in HDS catalyst prepa-

* Corresponding authors.
E-mail addresses: radost@ic.bas.bg, radostina.palcheva@yahoo.com (R. Palcheva), kaluza@icpf.cas.cz (L. Kaluža).

http://dx.doi.org/10.1016/j.apcata.2016.04.008
0926-860X/

rations has been found to be very efficient in an increasing number of Co (Ni)–Mo–S sites [28–40]. When a chelating agent, like citric acid, EDTA, or nitrilotriacetic acid (NTA) is added to the impregnation solution containing Co (or Ni) and Mo precursors, the formed Co(Ni)-chelating agent complex retards the sulfidation of the Co or Ni promoter until a more complete sulfidation of Mo, leading to an increased number of Co(Ni)–Mo–S sites, simultaneously suppressing the formation of bulk Co or Ni sulfides [28,30,31,33–36,38]. Ohta et al. studied the role of NTA, EDTA and CyDTA on CoMo, NiMo and NiW type catalysts [30]. They observed a positive effect of the organic molecule on the CoMo and NiW catalysts, and slightly less effect on the NiMo catalysts.

The use of thioglycolic acid (TGA) as a chelating agent in preparation of HDS catalysts has not been systematically studied up to now. The treatment of the CoMo oxidic phase with aqueous solution of thioglycolic acid was successfully applied to improve the performance of thiophene hydrodesulfurization catalysts [39]. Raman spectroscopy, EXAFS and XPS studies indicated that addition of TGA affected the sulfidation of the supported metals. A higher catalytic performance was attributed to the optimization of the nature and morphology of the active phase obtained by the use of this chelating agent which enabled to carry out a simultaneous sulfidation of both Co and Mo atoms [39].

The aim of the paper is to study the effect of both the mesoporous supports doped with niobium (Nb-SBA-15 and Nb-HMS) and the application of thioglycolic acid (TGA) as a chelating agent on catalytic performance of NiMo catalysts in HDS of 1-benzothiophene and thiophene at 350 °C.

2. Experimental

2.1. Synthesis of supports and catalysts

Nb-SBA-15 support was prepared as follows: Pluronic P123 (Aldrich, MW = 5800) (4.971 g) was dissolved on gentle heating in 145 mL of 1.6 M hydrochloric acid. After that, 11.2 mL of tetraethyl orthosilicate was added to this solution while mixing. Afterwards, the solution of 0.43 g of ammonium niobium oxalate (CBMM) in 8 mL of methyl alcohol was added. The mixture was put in a water bath with the temperature 45 °C and stirred for one day. The white suspension obtained was transferred to a Teflon lined autoclave and kept at 100 °C for 30 h. Then the content of the autoclave was filtered, washed extensively with water, dried and calcined at 600 °C in air for 8 h to liberate the organic template.

To prepare Nb-HMS, three solutions were prepared. The first contained 5.04 g of dodecylamine, 6.56 g of mesitylene, 2 mL of 1.6 M hydrochloric acid and 36.6 mL of ethanol. On slight heating and mixing, dodecylamine was dissolved and the true solution was obtained. The second solution contained 23 mL of tetraethyl orthosilicate and 20 mL of ethanol. The third solution was prepared from 0.879 g of ammonium niobium oxalate, which was dissolved in 23 mL of water. The second and third solutions were simultaneously added to the first solution under stirring. The stirring continued at 40 °C for 2 h and then the mixture was let stand at the laboratory temperature for 48 h. The precipitate was filtered, washed with water once and then several times with small portions of ethanol. The obtained cake was dried and calcined in air at 600 °C for 8 h. The Nb-SBA-15 and Nb-HMS materials showed Si/Nb atomic ratio 40.

The studied supports were impregnated with an aqueous solution of nickel nitrate ($Ni(NO_3)_2{\cdot}6H_2O$) and ammonium heptamolybdate. After the impregnation the obtained catalysts were dried at 120 °C and calcined at 400 °C in air flow. The nominal composition of the catalysts was 2.2 wt% Ni and 12 wt% Mo, reaching the molar ratio Ni/Mo = 0.3. The catalysts were labeled as NiMo/Nb-SBA-15 and NiMo/Nb-HMS.

Parts of the NiMo/Nb-SBA-15 and NiMo/Nb-HMS catalysts (dried at 120 °C and calcined at 400 °C) were treated with an aqueous solution of thioglycolic acid (TGA). The TGA:Mo molar ratio was 4.0. After 2 h of treatment, the so obtained solids were dried at 80 °C under N_2 for 15 h. These catalysts are labeled as TGA/NiMo/Nb-SBA-15 and TGA/NiMo/Nb-HMS.

The third series of catalysts were prepared by simultaneous impregnation of the supports with an aqueous solution of nickel nitrate, ammonium heptamolybdate and TGA. The catalysts were dried at 80 °C under N_2. They contained the same amounts of Ni and Mo as their calcined counterparts mentioned above. They were labeled as NiMoTGA/Nb-SBA-15 and NiMoTGA/Nb-HMS.

2.2. Catalyst characterization

The supports and NiMo catalysts were characterized by N_2 physisorption, small- and wide-angle XRD, acidity tests (TPD-NH_3, cumene cracking), SEM, UV–vis DRS, FTIR and XPS.

The textural properties of the supports and of the sulfided catalysts were investigated with a Micromeritics ASAP 2010 apparatus. Prior to the analysis, the oxide precursors were sulfided under the same conditions as described in the section on catalytic activity tests and evacuated at 105 °C for 12 h before the N_2 adsorption. Specific surface area and pore size distributions were determined from nitrogen adsorption–desorption isotherms at −195 °C, after drying the samples at 105 °C for 12 h and evacuation until the pressure 10^{-5} Pa was achieved (usually 2–5 h). To calculate the specific surface area (S_{BET}), the data were treated by the standard BET method. Total volume of mesopores V was determined from the amount of N_2 adsorbed at $P/P_0 = 0.98$. Surface area of mesopores (S_{meso}) and volume of micropores (V_{micro}) were calculated from t-plot according to Schneider [41].

The X-ray patterns of the supports, oxide precursors and fresh sulfided samples were recorded on a Bruker AXS 2D analyzer with filtered CuKα radiation (λ = 0.154056 nm) at 30 kV acceleration and 10 mA current of the X-ray tube, scan step 0.05° and 1 s accumulation time.

The scanning electron microscopy (SEM) was performed on a Philips SEM 515 apparatus, working at acceleration of 20 kV. The samples were covered with gold before putting them into the SEM chamber.

The DR UV–vis spectra were taken with a Thermo Evolution 300 spectrometer equipped with a Praying Mantis diffuse reflectance accessory.

The IR spectra of the samples mixed with KBr at approximately 1 wt% concentration were recorded on Nicolet 6700 FTIR spectrophotometer, Thermo Electron Corporation, USA, in 4000–400 cm^{-1} region at 0.4 cm^{-1} resolution accumulating 50 scans per spectrum. The XPS measurements of all samples were carried out in the analysis chamber of the electron spectrometer Escalab-MkII (VG Scientific) with a base pressure of $\sim 5 \times 10^{-8}$ Pa. The Nb_2O_5 and MoS_2 standards along with Nb-SBA-15 and Nb-HMS supports in powder form were pressed into sample holders, the pellets thus obtained had diameter of 10 mm and thickness of ~1 mm. The energy calibration was made by using C1s photoelectron line at 285.0 eV as a reference. The sulfided NiMo supported samples (400 °C, ramp 10 °C/min, 2 h, H_2S/H_2 1/10) were carefully mounted on scotch tape in order to avoid mechanical crushing of the particles. In this case, the energy reference was performed by taking O1s peak at 533.5 eV as a reference in order to avoid possible interference of the weak C1s signal from the samples surface with the stronger one arising from the scotch tape. The C1s, O1s, Si2p, Nb3d, Mo3d, Ni2p and S2p photoelectron lines were recorded and the surface compositions were evaluated by using the normalized pho-

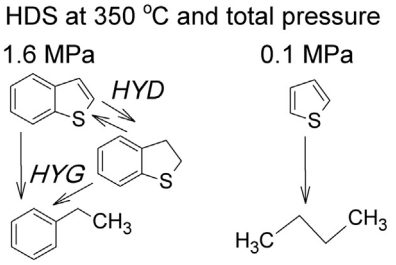

Fig. 1. Schemes of hydrodesulfurization (HDS) of 1-benzothiophene and thiophene: (HYD) hydrogenation of 1-benzothiophene to dihydrobenzothiophene, (HYG) hydrogenolysis of the benzothiophenes to ethylbenzene.

toelectron intensities obtained through dividing the peak areas by the corresponding photo ionization cross sections taken from Scofield [42].

2.3. Catalytic activity

The hydrodesulfurization of 1-benzothiophene (BT) was performed in the gas phase using an integral fixed-bed tubular flow microreactor (i.d. 3 mm) at 350 °C and 1.6 MPa. Prior to the measurements, the catalysts were sulfided in situ with an H_2S/H_2 flow (1/10) at 400 °C and atmospheric pressure with a temperature ramp of 10 °C/min and a dwell time of 1 h. The composition of the feed was kept constant at 16 kPa, 200 kPa and 1384 kPa of 1-benzothiophene (BT), decane and hydrogen, respectively. The catalyst sample (0.03 g) was diluted with an inert α-Al_2O_3 with particle size fraction 0.16-0.32 mm to form a bed length of 30 mm. The reaction was run at three feed rates of BT including 7.7 mmol h^{-1}, 10.3 mmol h^{-1} and 15.5 mmol h^{-1}. The steady state was reached in 30 min after each change in the feed rate. No changes of conversions during the following 1 h were observed. The reaction mixture was analyzed on a Hewlett–Packard gas chromatograph (6890 series) equipped with a capillary column (HP-5, 30 m, 0.53 mm, 1.5 μm). Dihydrobenzothiophene (DH) and ethylbenzene (EB) were identified in the reaction products. The scheme of BT HDS is shown in Fig. 1. The relative compositions a(BT), a(EB) and a(DH), BT conversion x(BT) and EB and DH yields, y(EB), and y(DH) were defined as $a(BT) = (1 - x(BT)) = n(BT)/n_0(BT)$, $a(EB) = y(EB) = n(EB)/n_0(BT)$, $a(DH) = y(DH) = n(DH)/n_0(BT)$, where $n_0(BT)$, n(BT), n(EB), and n(DH) were the initial number of moles of BT, final number of moles of BT, EB, and DH, respectively. The rate constant of EB formation, k(EB), was calculated using an empirical pseudo-first-order rate equation ($a(EB) = 1 - \exp(-k(EB)W/F)$). An example how relative composition depends on space time W/F and how k(EB) was obtained is given in Fig. 2.

The industrial $NiMo/Al_2O_3$ catalyst KF 846 (Albemarle, The Netherlands, 3.1wt% NiO, 20.7wt% MoO_3, S_{BET} (oxidic state) = 253 m^2 g^{-1}) was used as a reference catalyst in HDS of 1-benzothiophene.

The hydrodesulfurization of thiophene (TH) was measured in a continuous flow micro- reactor at 350 °C at atmospheric pressure. The catalyst sample (0.1 g) was mixed with SiC (size 83 μm) to obtain a bed length of 75 mm. The catalyst was activated by sulfidation as it was described above. After the completion of the activation, the catalyst was flushed out with argon for 30 min. Then, feeding of the reaction mixture (6 vol% of thiophene in hydrogen) at WHSV 3.2 h^{-1} was started. The steady state was reached 3 h after the start of the reaction. During the following 2 h of the catalytic experiment, no change in conversion was observed. The conversion of thiophene x(TH) was determined by means of a gas chromatograph equipped with a thermal conductivity detector (TCD). It was defined as $x(TH) = n(TH)/n_0(TH)$, where $n_0(TH)$ and n(TH) were initial and final number of moles of TH, respectively. The rate constant

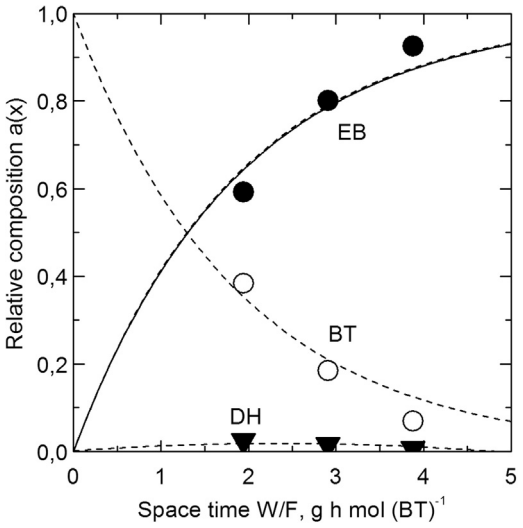

Fig. 2. Hydrodesulfurization of 1-benzothiophene over NiMoTGA/Nb-SBA-15 catalyst: (open circles) benzothiophene, (filled triangles) dihydrobenzothiophene, (filled circles) ethylbenzene, (dash lines) the curves calculated using a scheme of four pseudo-first-order reaction from Fig. 1, (solid line) the curve calculated using an empirical pseudo-first-order rate equation (see text).

of thiophene conversion was k(TH) calculated using an empirical pseudo-first-order rate equation.

The cumene cracking was tested at 400 °C and 0.5 MPa in an integral tubular-flow microreactor with fixed bed of the catalysts [43]. The sample charge (0.02 g) was in situ activated by H_2 at 400 °C for 0.5 h. Gas chromatograph Agilent 4890D operated with flame ionization detector and 30 m capillary DB-5 column (0.25 mm) was used for determination of cumene conversion to benzene and propane. Nevertheless, none of the studied samples (supports or catalysts) exhibited activity in the cumene cracking reaction. Thus, we can state the studied sulfide catalysts possessed some acidity but not so strong that they would crack the cumene under conditions applied during catalytic tests (reaction temperature 400 °C).

3. Results and discussion

3.1. Structural and textural properties of the supports and catalysts

Table 1 summarizes the textural properties (BET surface area, pore volume and S_{meso}) of the supports and sulfided NiMo catalysts as well as HDS activity. The acid properties of the sulfided NiMo catalysts were analyzed by TPD of ammonia (NH_3-TPD, Supplementary content) and the total concentration of acid sites between 25 °C to 500 °C was calculated as the amount of ammonia adsorbed per gram of catalyst (Table 1).

After sulfidation, the surface areas of catalysts varied in the range of 410–570 m^2 g^{-1} (Table 1). The N_2 adsorption desorption isotherms and pore-size distributions of the supports and the corresponding NiMo sulfided catalysts are shown in Fig. 3 and Fig. 4. The isotherms are of type IV, characteristic of the mesoporous materials. According to the IUPAC classification, the hysteresis loops of the Nb-SBA-15 and the Nb-HMS can be classified as H1 and H3 types, respectively [44]. In all of the cases, the isotherms and pore-size distribution curves of the NiMo catalysts maintain identical features like those of the supports (Fig. 4).

The Nb-HMS support exhibit a maximum in the pore-size distribution curves closer to the micropore region than Nb-SBA-15 (Fig. 3). For this reason, Nb-HMS shows higher values for S_{BET} and S_{meso} than Nb-SBA-15 (Table 1). After deposition of NiMo active components on Nb-HMS, due to partial blocking of small pores by

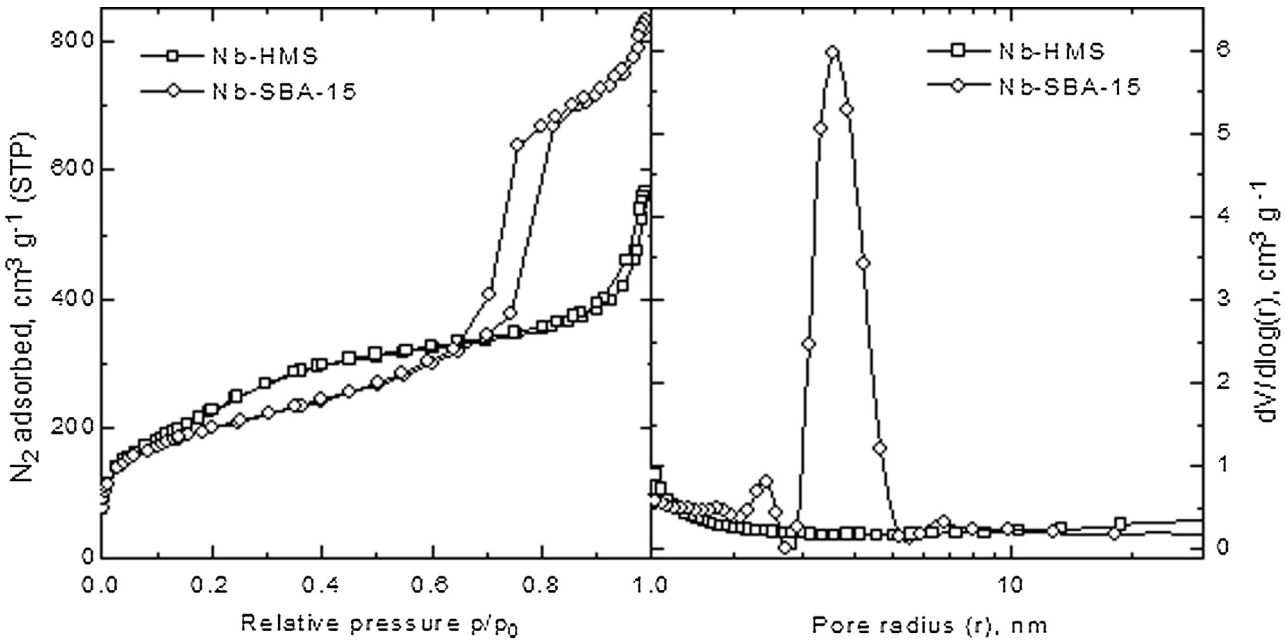

Fig. 3. Isotherms and pore-size distributions of the Nb modified mesoporous supports.

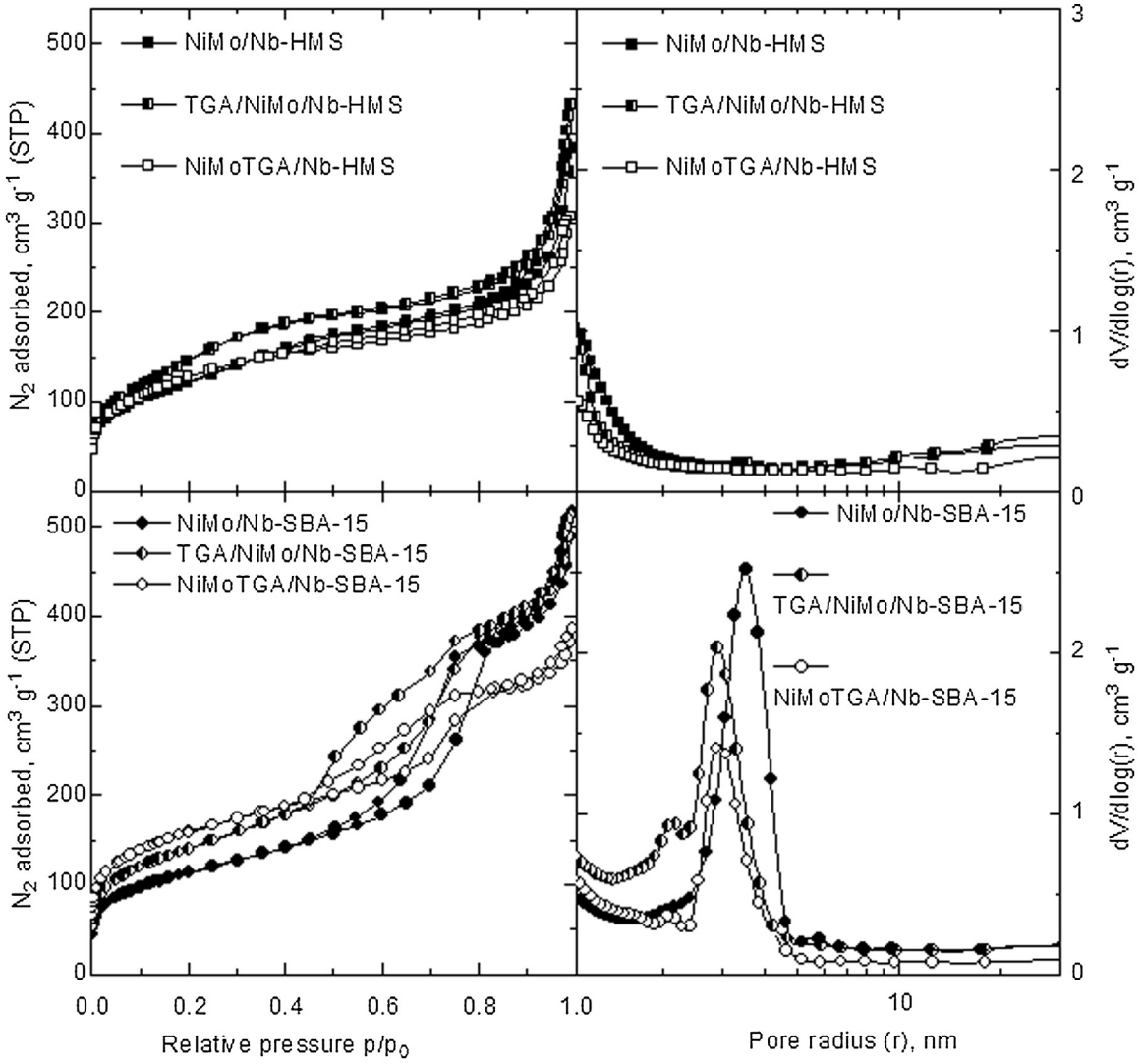

Fig. 4. Isotherms and pore-size distributions of the Nb-HMS and Nb-SBA–15 supported sulfide NiMo catalysts.

Table 1
Textural properties of the supports and prepared NiMo catalysts, their acidities and activities in HDS.

Sample	S_{BET} $m^2\ g^{-1}$	V_{meso} $cm^3\ g^{-1}$	V_{micro} $cm^{3\,g-1}$	S_{meso} $m^2\ g^{-1}$	NH_3[d] mmol/g	k(EB)[a]	k (TH)[b]
Nb-HMS	835	0.99	0.15	643	–	–	–
NiMo/Nb-HMS	439	0.61	0.08	296	0.70	258	1130
TGA/NiMo/Nb-HMS	538	0.75	0.09	421	–	164	460
NiMoTGA/Nb-HMS	464	0.49	0.08	327	0.42	388	1033
Nb-SBA-15	714	1.38	0.15	429	–	–	–
NiMo/Nb-SBA-15	507	0.83	0.10	324	0.87	232	940
TGA/NiMo/Nb-SBA-15	410	0.83	0.08	261	0.73	461	1340
NiMoTGA/Nb-SBA-15	570	0.56	0.13	327	0.66	530	1679
$NiMo/Al_2O_3$ Ref. KF846	–	–	–	–	–	473[c]	–

[a] mmol (EB) $g_{(ex\text{-}situsulfidedcatalyst)}^{-1}$ h.
[b] mmol (TH) g_{cat}^{-1} h.
[c] Normalized per gram of catalyst in oxidic state (sulfide may exhibit higher activity to some extent).
[d] Prior to the measurements, the catalysts were heated to 350 °C at a rate of 20 °C min.

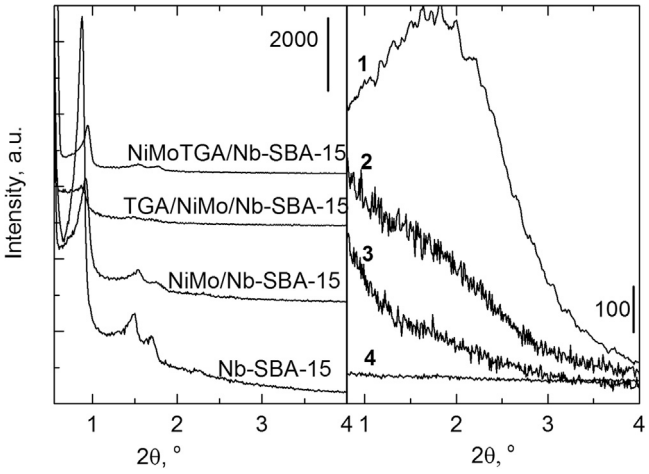

Fig. 5. Small XRD patterns of the supports and NiMo catalysts: 1-Nb-HMS, 2-NiMo/Nb-HMS, 3-TGA/NiMo/Nb-HMS, 4- NiMoTGA/Nb-HMS.

the introduced active phase, the S_{BET} and S_{meso} were reduced to a higher extent than those on Nb-SBA-15.

Interestingly, a sequential treatment of the NiMo catalysts by thioglycolic acid (TGA/NiMo samples) leads to the increased S_{BET} and S_{meso} of Nb-HMS-supported catalyst while S_{BET} and S_{meso} of the Nb-SBA-15 supported catalysts were decreasing. It was suggested, that a part of the NiMo phase in NiMo/Nb-HMS was deposited outside of the pores. Being treated with TGA these species were prone to releasing Mo ions to form a three dimensional Mo complex with TGA, which led to the formation of crystals of Mo_9O_{26} in TGA/NiMo/Nb-HMS sample (JCPDS no. 12-0753) registered by XRD (Fig. 6).

The size of Mo_9O_{26} crystalline phase was calculated by the use of the Scherrer equation at the reflection angle 22.054° possessing the value 10 nm.

In contrast to the conventionally prepared catalyst (samples NiMo), a simultaneous co-impregnation of the supports with Ni, Mo and TGA (samples NiMoTGA) leads to systematical increase of the S_{BET} and S_{meso} meanwhile keeping an X-ray amorphous character of the active phase (Fig. 6). Additionally, it can be concluded that for all studied methods of deposition, the large mesoporous structure of Nb-SBA-15 was more convenient for the NiMo catalyst preparation.

A small-angle XRD of the supports and catalysts is shown in Fig. 5. The X-ray powder patterns, recorded in the 2θ interval 0.5–6°, showed reflections at 2θ = 1.98° for Nb-HMS and at 2θ = 0.85, 1.42 and 1.69 with (*hkl*) indexes (100) (110) and (200) for Nb-SBA-15, respectively. The XRD pattern of the Nb-SBA-15 sample is characteristic for the *p6mm* hexagonal structure [45]. However, the reflection at 2θ = 1.98 for Nb-HMS sample showed that this material is not well ordered. After deposition of NiMo onto the Nb-SBA-15, the structure remained, with small shift of the peaks to higher 2θ values, more or less unaltered. The oxide form of calcined NiMo catalyst supported on Nb-SBA-15 showed lower intensity of the reflections as compared to that of the starting Nb-SBA-15 support. The reduction in the reflection intensities can be explained by some distortion of hexagonal arrangement and destruction of channels in the starting supports due to deposition of dispersed Ni-Mo oxides inside the channels.

With regard to the XRD in the wide-angle region (Fig. 6), the patterns of NiMo/Nb-SBA-15 and TGA/NiMo/Nb-SBA-15 catalysts are very diffusive and analyzing them it could not be excluded the minor presence of some orthorhombic MoO_3 phase with the reflections at 2θ = 22.57, 25.90 and 32.29 (ICSD Ref. Code 98-064-4058) and α-$NiMoO_4$ phase with the reflections at 2θ = 12.71, 22.57 and 42.70 (ICSD Ref Code 98-008-1059) in highly dispersed form (Fig. 6). This suggestion was confirmed later by the UV–vis DRS and FTIR spectra of the catalysts (Figs. 8 and 9).

3.2. SEM of supports

Fig. 7 shows the SEM pictures of Nb modified mesoporous materials. The figure of Nb-SBA–15 shows a typical wormhole structure while Nb-HMS demonstrates a non-uniform structure containing both small and rough particles.

3.3. UV–vis DR spectra

Fig. 8 shows the diffuse reflectance UV–vis spectra of pure Nb_2O_5, niobium modified mesoporous supports (Nb-SBA-15 and Nb-HMS) and supported NiMo catalysts. The broad band at 300–400 nm occurring for Nb_2O_5 oxide is caused by $O^{2-} \rightarrow Nb^{5+}$ charge transfer (Fig. 8A). The Nb-SBA-15 sample shows main absorption band at 234 nm due to the ligand-to-metal charge transfer in Nb species (Td) [46]. The absence of the broad band at 300–400 nm reveals that the niobium oxide species are mainly in tetrahedral positions and no extra framework crystalline Nb_2O_5 phase exists in the Nb-SBA-15 sample. In contrast, the presence of the band at 307 nm along with the band at 234 nm in the Nb-HMS sample is an indication that the Nb_2O_5 species and isolated Nb species in tetrahedral coordination coexist on the support.

The calcined NiMo/Nb-SBA-15 and NiMo/Nb-HMS catalyst show bands at 238, 260–280 range and 700 nm (Fig. 8 B,C). The bands in the 260–280 nm range are due to $O^{2-} \rightarrow Mo^{6+}$ ligand-to-metal charge transfer transition (LMCT) in tetrahedral coordination of isolated molybdate species (MoTd); moreover, second absorption band at about 230 cm^{-1} is indicative of the coexistence of a mixture

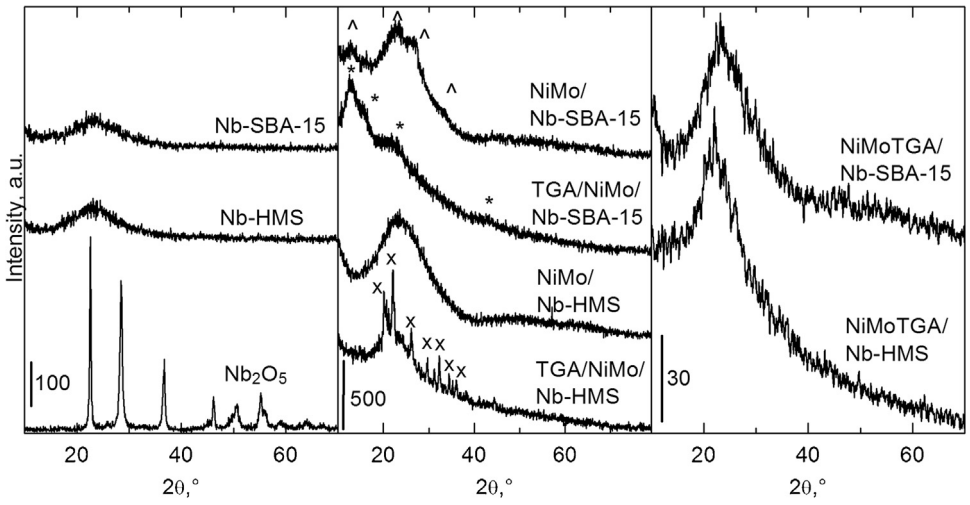

Fig. 6. Wide angle XRD patterns of the supports and NiMo catalysts: (x) Mo_9O_{26}. (*) $NiMoO_4$, (^) MoO_3

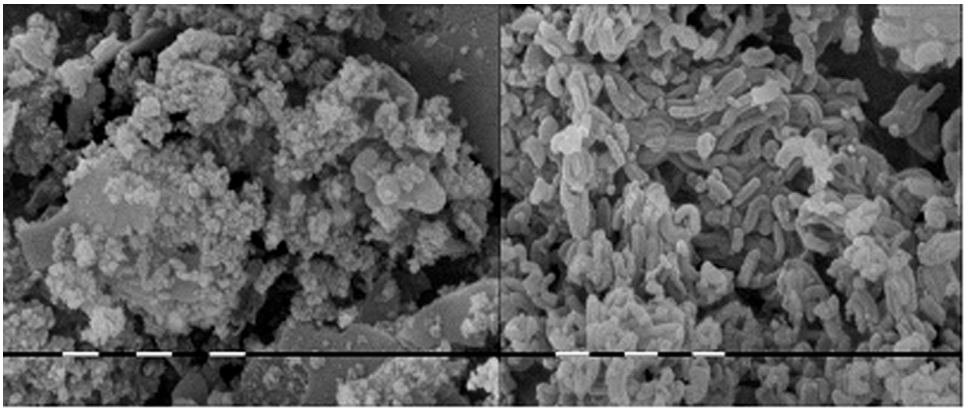

Fig. 7. SEM picture of Nb-HMS (left) and Nb-SBA-15 (right), magnification 10000, bar 1 μm.

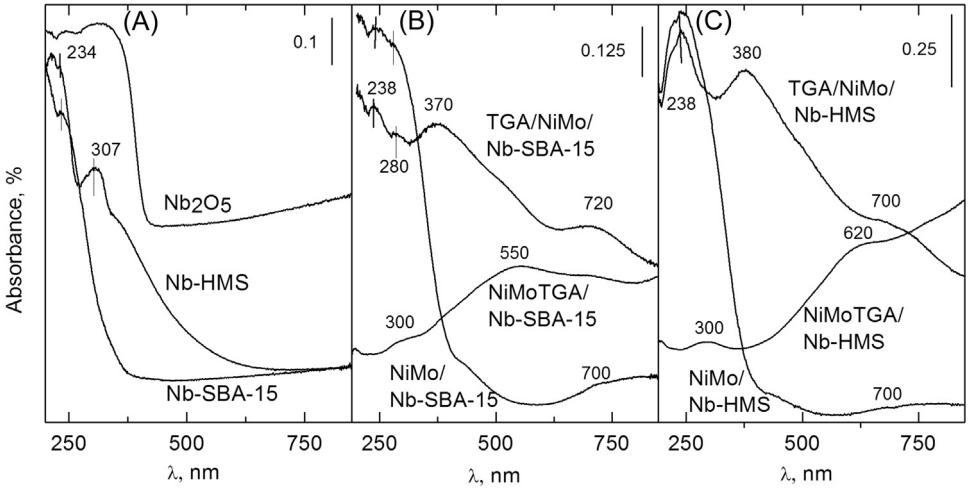

Fig. 8. UV–vis DRS spectra of Nb_2O_5 and the supports (A) and NiMo catalysts prepared on Nb-SBA-15 (B) and Nb-HMS (C).

of Mo^{6+} species in octahedral and tetrahedral coordination [47]. The band at 700 nm is characteristic of the Ni^{2+} ions in Oh symmetry interacting with molybdenum oxo-species [48]. Addition of thioglycolic acid to the NiMo catalysts substantially changes their UV–vis DRS spectra. When TGA acid was added to the calcined NiMo catalysts, the bands at 238, 280 and 700 nm were still observed (Fig. 8 B,C), however, a new band with high intensity at 300–380 nm appeared. Gutierrez et al. assigned this band to formation of polymolybdate octahedral (Oh) Mo species [47]. Considering our XRD results (Fig. 6) this band can tentatively be attributed to the presence of small MoO_3 clusters in TGA/NiMo/Nb-SBA-15 sample and Mo_9O_{26} crystalline phase formed in TGA/NiMo/Nb-HMS sample.

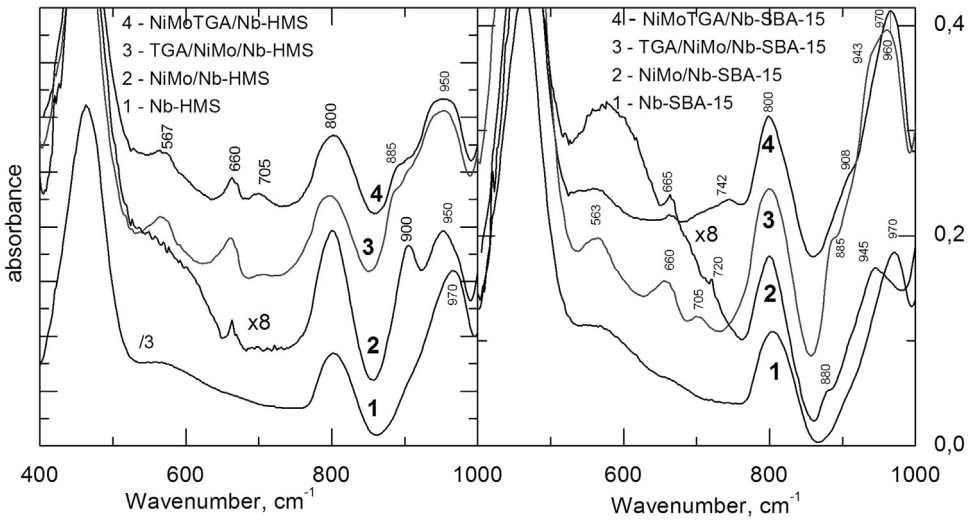

Fig. 9. FTIR spectra of Nb-SBA-15 and Nb-HMS supports and of the NiMo catalysts.

In the case of the catalysts prepared by the simultaneous impregnation (NiMoTGA/Nb-SBA-15 and NiMoTGA/Nb-HMS samples) the UV–vis DRS band at 300 nm has a very low intensity, which points out to a better dispersion of octahedral Mo species. A broad band at 550–600 nm was also detected, which characterizes, most probably, the complex of the Mo and/or Ni atoms with TGA.

It is well known that thioglycolic acid forms complexes with molybdenum by chelating the metal via the SH and COOH groups [49–51].

3.4. FTIR spectra

The IR spectra of the synthesized samples in the region of 400–1000 cm^{-1} are presented in Fig. 9. Exact assignment of the bands to specific compounds is very difficult, as bands of different compounds overlap. Nevertheless, in the spectra of Nb-SBA-15 and Nb-HMS supports, essential IR bands were observed at 460 and 800 cm^{-1}. These bands correspond to the vibrations of Si—O—Si bonds [52]. The band at 970 cm^{-1} in the Nb-modified supports is attributed to the perturbed Si—O stretching vibration of the silica framework by the incorporated neighboring metal ion and formation of Si—O—Me bonds [53]. The plateau at 550–600 cm^{-1} can be connected with the presence of Nb—O—Nb bond in the support.

The calcined supported NiMo catalysts showed change in their spectra in comparison with the spectra of the supports: bands at ~660, 880–900, 945–950 cm^{-1} were observed in both catalysts. The absorption bands at 880–900 cm^{-1} are ascribed to $(MoO)_4^{2-}$ tetrahedra [54], while the band at 950 cm^{-1} is attributed to vibrations of Mo = O bonds in Mo octahedra of high polymerized compounds. The other characteristic bands of MoO_3 (611 and 875 cm^{-1}) ascribed to Mo–O–Mo [55] are not too distinct in the IR spectra of both samples, what indicates that MoO_3 is well dispersed. A shift of the ~970 cm^{-1} band in the mesoporous supports to 945–950 cm^{-1} in NiMo catalysts could indicate weaker bonding of the Mo–O species with silica.

After the treatment of the calcined NiMo catalysts with TGA, the intensity of bands previously observed in the supported NiMo catalysts (belonging to SiO_2 and MoO_3) was increased and a new band at 705 cm^{-1} were observed in the spectra of TGA/NiMo/Nb-SBA-15 sample. The bands at ~660, 705, sh943 cm^{-1}, 960 cm^{-1} characteristic of $NiMoO_4$ phase are more visible in the spectra of the TGA/NiMo/Nb-SBA-15 catalyst which is consistent with the XRD data (Fig. 6).

The NiMo catalysts prepared by a simultaneous co-impregnation of the supports with Ni, Mo and TGA (dried at 80 °C) showed, in principle, the IR spectra similar to those of the other catalysts. It should be noted the appearance of a broad band at 742 cm^{-1} in NiMoTGA/Nb-SBA-15 sample: Mo in the bridge Mo—O—Mo bonds could be replaced with Ni forming substituted Ni–O–Mo species.

3.5. XPS of sulfided catalysts

The surface compositions in atomic percents for niobium modified silica supports along with those for NiMo samples in oxidic and sulfided form are presented in Table 2. The Si/Nb atomic ratio is 130 for the Nb-HMS support and 65 for the Nb-SBA-15, i.e. for both samples considerably higher than the expected value of 40. The corresponding peak binding energies are shown in Table 3 with values for MoS_2 and Nb_2O_5 standards. The $Nb3d_{5/2}$ binding energy for Nb-SBA-15 support is closer to that for the Nb_2O_5 standard and even lower. Possible explanation of this fact is the existence of niobium containing particles on the SBA-15 surface, which might be partially reduced due to the X-ray irradiation in vacuum. The amount of niobium on the sulfided surface is lower by factor of ~2 as compared to that before sulfidation. It is suggested by Faro Jr. et al. [12], that there is strong interaction of nickel and molybdenum with niobium on the surface. This could explain in some extent the lower amount of niobium for NiMo supported samples, if one assumes the preferential grafting of nickel and molybdenum on niobium containing species. The total amount of molybdenum as revealed by XPS is lower as compared to the loaded one during impregnation. Calculations from Table 2 on the amount of molybdenum on the surface is about 5wt.%, i.e. considerably lower than the loaded 12wt.%. Furthermore, the Mo/Ni weight ratios, calculated from Table 2 is ~7.5 (at.% ratio) × 95.9/58.7 ≈ 12 (wt.% ratio), which is higher than the loaded value of 3 (here, 95.9 and 58.7 are the atomic masses of Mo and Ni respectively). These low amounts of niobium, molybdenum, nickel and respectively sulfur make difficult spectra processing. The Mo3d, Nb3d, S2p and Ni2p spectra for NiMo/Mb-SBA-15 sample are shown on Fig. 10a–c. The degree of sulfidation is about 72% calculated as Mo3d (MoS_2) peak area of the total Mo3d one. The sulfur spectrum exhibits peak positions typical for sulfides. It is worth to note that there is no peak features around 169 eV, characteristic of sulfate (SO_4^{2-}) groups. The Nb3d line is weak, so the peak fitting was performed for illustration purposes only. The situation is similar for the Ni2p spectrum, where only peak area was evaluated in

Table 2
Surface composition (in at.%) of Nb-HMS, Nb-SBA-15 supports, NiMo/Nb-HMS, NiMo/Nb-SBA-15 samples in 'as prepared' form and after sulfidation.

Elements Photoelectron lines	O O1s	Si Si2p	Ni Ni2p	S S2p	Mo^{4+} Mo3d	MoS_xO_y Mo3d	Mo^{6+} Mo3d	Nb Nb3d
Supports								
Nb-HMS	62.9	36.8	–	–	–	–	–	0.28
Nb-SBA-15	64.4	35.0	–	–	–	–	–	0.54
Samples before sulfidation								
NiMo/Nb-HMS	63.2	35.8	0.15	–			0.71	0.19
TGA/NiMo/Nb-HMS	61	28.4	0.17	9.6			0.64	0.15
NiMoTGA/Nb-HMS	60.1	28.3	0.62	9.5			1.28	0.15
NiMo/Nb-SBA-15	63.9	33.8	0.31	–			1.6	0.44
TGA/NiMo/Nb-SBA-15	61.9	32.6	0.18	4.4			0.46	0.45
NiMoTGA/Nb-SBA-15	62.9	32.1	0.36	3.33			0.86	0.36
Sulfided samples								
NiMo/Nb-HMS	61.3	36.3	0.12	1.36	0.69	0.09	0.06	0.13
TGA/NiMo/Nb-HMS	61.9	35.8	0.11	1.25	0.69	0.10	0.10	0.10
NiMoTGA/Nb-HMS	60.8	36.1	0.16	1.75	0.90	0.17	0.11	0.07
NiMo/Nb-SBA-15	61.3	36.1	0.12	1.26	0.69	0.14	0.10	0.26
TGA/NiMo/Nb-SBA-15	61.8	36.2	0.10	0.97	0.50	0.10	0.07	0.28
NiMoTGA/Nb-SBA-15	61.2	36.4	0.12	1.18	0.72	0.14	0.13	0.20

Table 3
Photoelectron peak positions in eV (±0.1 eV) for Nb_2O_5, MoS_2 standards, Nb-HMS, Nb-SBA-15, TGA/Nb-SBA-15 supports, NiMo supported samples in 'as prepared' and in sulfided forms.

Photoelectron peak	O1s	Si2p	$Ni2p_{3/2}$ (main line) oxide	$S2p_{3/2}$	Mo3d5/2(MoS_2)	$Nb3d_{5/2}$
Standards						
Nb_2O_5	530.4[a]	–	–	–	–	207.4
MoS_2	–	–	–	162.7*	229.8	–
Supports						
Nb-HMS	533.3[a]	104.0	–	–	–	208.6
Nb-SBA-15	533.3[a]	103.9	–	–	–	207.1, 208.6
TGA/Nb-SBA-15	533.3[b]	104.1	–	164.5	–	207.9
Samples before sulfidation						
NiMo/Nb-HMS	533.3[b]	104.0	856.6	–	232.6	208.4
TGA/NiMo/Nb-HMS	533.3[b]	104.0	856.6	164.2	232.6	208.3
NiMoTGA/Nb-HMS	533.3[b]	104.0	856.6	164.0	232.2	208.5
NiMo/Nb-SBA-15	533.3[b]	104.0	856.6	–	232.9	207.5
TGA/NiMo/Nb-SBA-15	533.3[b]	104.0	856.6	164.6	232.9	207.8
NiMoTGA/Nb-SBA-15	533.3[b]	104.0	856.8	164.5	232.5	207.7
Sulfided samples			$Ni2p_{3/2}$ (main line)sulfide			
NiMo/Nb-HMS	533.3[b]	104.0	854.2	162.1	229.3	208.3
TGA/NiMo/Nb-HMS	533.3[b]	103.9	854.1	161.7	228.9	207.0
NiMoTGA/Nb-HMS	533.3[b]	104.0	853.9	161.9	229.1	207.4
NiMo/Nb-SBA-15	533.3[b]	104.0	853.8	161.9	229.1	207.7
TGA/NiMo/Nb-SBA-15	533.3[b]	104.0	853.8	161.8	229.1	207.4
NiMoTGA/Nb-SBA-15	533.3[b]	104.1	853.6	162.1	229.3	207.7

[a] Energy scale calibrated by using C1s peak at 285.0 eV as a reference.
[b] Energy scale calibrated by using O1s peak at 533.3 eV as a reference.

order to estimate the nickel surface concentration. The degree of sulfidation of nickel for different samples is estimated to be in the range 50–70%.

3.6. TPD-NH_3 of sulfided catalysts

The total acidity for the NiMo/Nb-mesoporous silica supported catalysts followed the order of NiMo/Nb-SBA-15 > NiMo/Nb-HMS and meets values in the range of 0.4–0.9 mmol/g (Table 1 and Supplementary content). The treatment of the calcined supported NiMo/Nb-SBA-15 catalyst by TGA lowered the acidity by ~20% (Table 1). When TGA was added simultaneously with Ni and Mo components to the supports, next trend in the total acidity order of both kinds of the catalyst sets can be seen: NiMo > TGA/NiMo > NiMoTGA. In general, any addition of TGA to the NiMo catalysts lowered the acidity, the common addition of active components and TGA impaired the acidity most. Probably, acidic sites of the supports, serving as anchoring sites for immobilization, are gradually neutralized by deposed active components and TGA. Catalytic activity in HDS reaction of 1-benzothiophene seems to be only roughly dependent on the acidity of the catalyst. Evidently, the acidity is not the main factor, determining the HDS activity of catalysts.

3.7. HDS activity of NiMo catalysts

The empirical pseudo-first-order rate constants of the ethylbenzene formation k(EB) were calculated from the dependence of the reaction mixture composition on the space velocity and used as an index of the catalyst activity in HDS of 1-benzothiophene. The empirical pseudo-first-order rate constants of thiophene conversion were calculated as an index of catalyst activity in HDS of thiophene. The HDS activities are summarized in Table 1. Selectivity to the ethylbenzene (EB) and dihydrobenzothiophene (DH) formation during the 1-benzothiophene HDS is expressed as a dependence of y(EB) and y(DH), respectively, on x(BT) in Fig. 11.

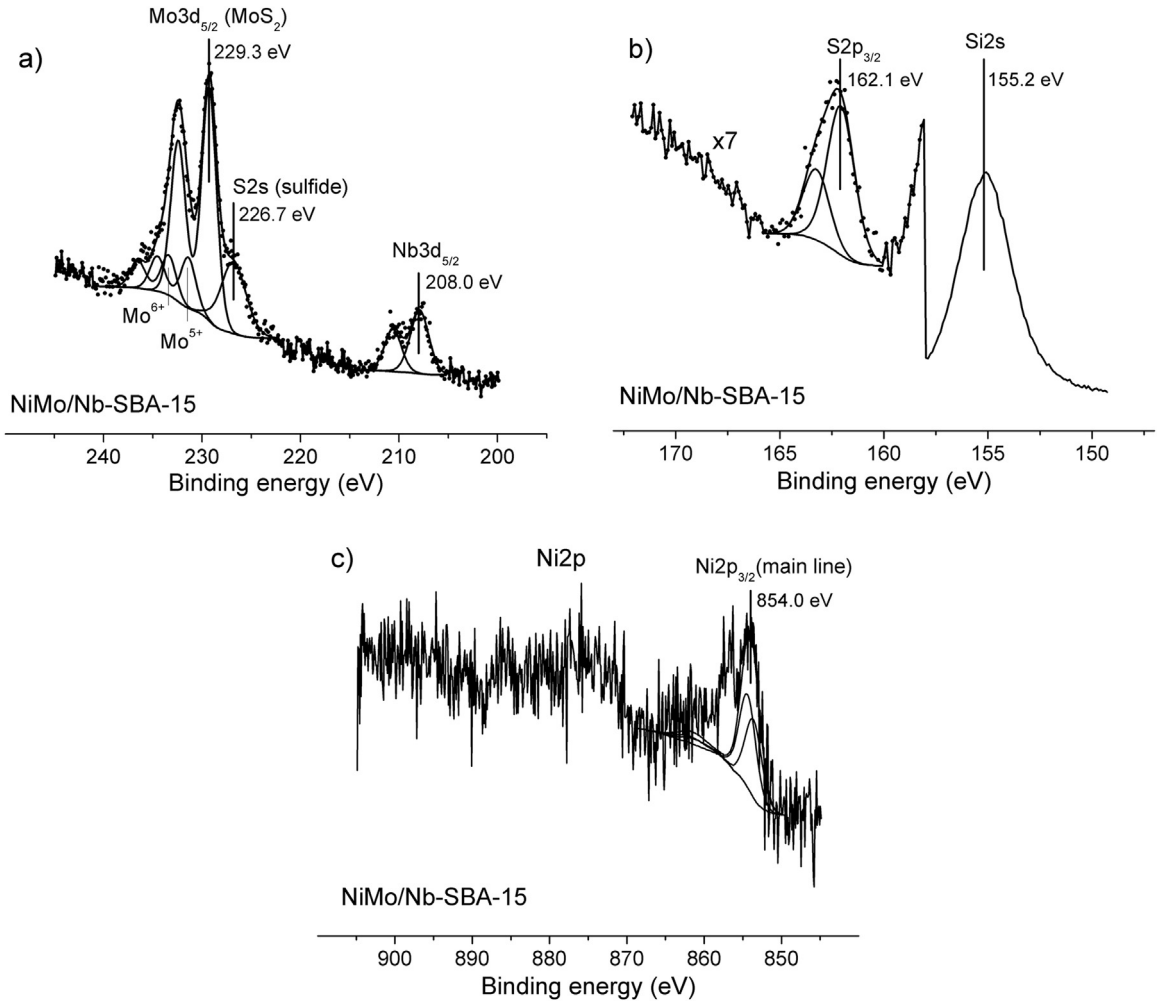

Fig. 10. XPS a) Mo3d, S2s, Nb3d, b) S2p, Si2s, c) Ni2p lines for sulfided NiMo/Nb-SBA-15 sample.

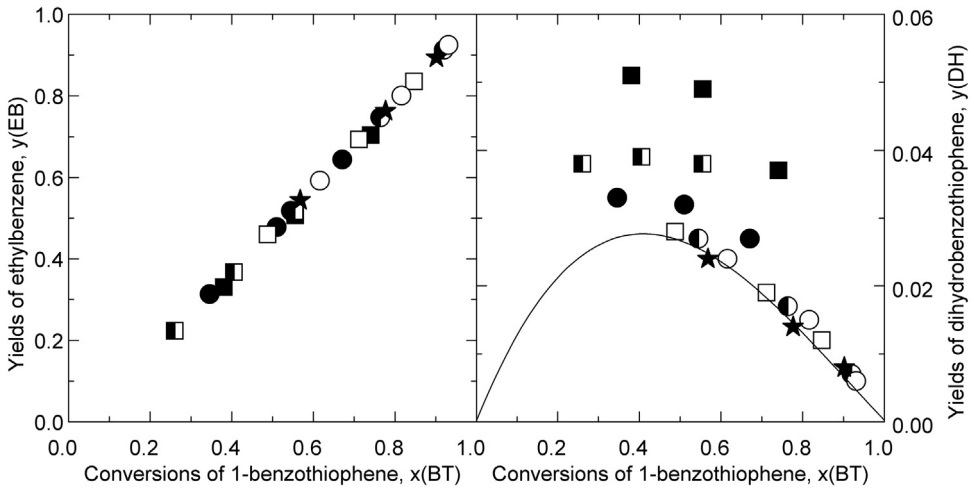

Fig. 11. Selectivity to ethylbenzene (EB) and dihydrobenzothiophene (DH) during the 1-benzothiophene (BT) hydrodesulfurization: (squares) Nb-HMS supported catalysts, (circles) Nb-SBA-15 supported catalysts, (filled squares and circles) NiMo catalysts, (half–filled squares and circles) TGA/NiMo catalysts, (open symbols) TGA assisted co–impregnation i.e. NiMoTGA catalysts, and (stars and solid line) reference industrial catalyst $NiMo/Al_2O_3$.

For the Nb-HMS supported catalysts, the HDS activity decreased when calcined NiMo catalysts were treated with thioglycolic acid. In contrast, the activity was increased by the factor 1.5 when TGA was added to the supports by the simultaneous impregnation method. The diffraction lines corresponding to the reflections of Mo_9O_{26} phase can be observed in the XRD pattern of TGA/NiMo/Nb-HMS sample indicating that there is a poor dispersion of the Mo phase on the surface when the calcined NiMo catalysts were impregnated with TGA.

It was suggested that the highly microporous systems of Nb-HMS were prone to release Mo phase while treating the calcined catalysts NiMo/Nb-HMS catalysts with TGA. Mo_9O_{26} practically corresponds to slightly oxygen deficient MoO_3. The oxygen defects could have been induced by organic agent—TGA, which might cause partial reduction of the molybdenum oxide. The released species formed three-dimensional phase (Fig. 6), which led to low HDS activities after sulfidation. The XRD spectra of the sulfided catalysts (Supplementary content, Fig. 6S) are rather diffuse, what means that sulfides are nano-dispersed and not well crystallized. The positions of the most intensive reflections of MoS_2 are indicated (JCPDS no. 37-1492, $2\theta = 14^\circ$, 33.2°, 58.6°). Additionally, the possible reflections from rhombohedral Ni_3S_2 is showed at $2\theta = 21.8^\circ$, 31.1°, 37.8°, 44.4°, 50.1°, 55.3° (JCPDS no. 44-1418). According to this analysis, most dispersed are sulfides formed in NiMoTGA/Nb-SBA-15 and TGA/NiMo/Nb-SBA-15 catalysts and less dispersed in NiMoTGA/Nb-HMS and TGA/NiMo/Nb-HMS catalysts.

Compared to the NiMo/Nb-HMS catalyst, the HDS activity of the NiMo/Nb-SBA-15 catalyst (Table 1) increased more than two times upon treatment with TGA. The statement is valid for both kinds of catalysts, the one prepared by the post-treatment of NiMo/Nb-SBA-15 with TGA, i.e. TGA/NiMo/Nb-SBA-15 and the catalyst prepared by the simultaneous impregnation of the support with Ni, Mo and TGA, i.e. NiMoTGA/Nb-SBA-15. It is suggested that the large mesoporous systems of the support in addition to the formation of $NiMoO_4$ species (XRD, FTIR results) which promote the HDS reaction [56] were crucial for keeping the NiMo phase dispersed and active on the TGA/NiMo/Nb-SBA-15 sample.

Nonetheless, the direct co-impregnation method (Ni, Mo and TGA) used for NiMoTGA/Nb-SBA-15 led to the highest HDS activity among the studied catalysts including the reference KF 846, which is Al_2O_3-supported one. Very likely, simultaneous impregnation method leads to formation of complexes of Ni, Mo and TGA (UV–vis DRS results) with the result of finely dispersed Ni–Mo–S phase. No crystalline phases are detected in the XRD pattern of NiMoTGA/Nb-HMS and NiMoTGA/Nb-SBA-15 samples (Fig. 6), suggesting that the Ni and Mo species are well dispersed on the surface of the mesoporous materials, when the catalysts were prepared by simultaneous impregnation method.

Concerning the catalysts prepared by the TGA treatment of NiMo supported catalysts, both catalysts show a different behavior in the HDS reaction, because the state of niobium in the two supports differs. In Nb-HMS, niobium exists in isolated tetrahedral coordination and as Nb_2O_5 species dispersed on the support surface (UV–vis DRS results). However, niobium in the second catalyst supported over Nb-SBA-15 is located only in isolated tetrahedral coordination in the framework positions (Fig. 8A). Different positions of niobium evolve a different action in the HDS reaction. It was suggested that in the case of the TGA/NiMo/Nb-HMS catalyst the sulfidation of the catalyst components proceeds separately, niobium sulfidation proceeds first and then is followed by the activation of molecular hydrogen which affects the arising MoS_2 via spillover. In the case of TGA/NiMo/Nb-SBA-15, where Nb is embedded in the framework, sulfidation of NiMo proceeds conventionally forming Ni–Mo–S active phase. Cedeño et al. [57] reported that incorporation of Nb to the silica framework leads to Nb species that are easily reducible but more difficult to sulfide than polymerized or agglomerated Nb_2O_5. These changes are reflected in the HDS activity of the samples.

Selectivity to the dihydrobenzothiophene (DH) formation during HDS of 1-BT (Fig. 11) was low indicating a good promotion of Mo phase by Ni. In detail, the most active NiMoTGA/Nb-HMS, TGA/NiMo/Nb-SBA-15 and NiMoTGA/Nb-SBA-15 catalysts showed practically the same and low selectivity to DH as the reference $NiMo/Al_2O_3$ industrial catalyst. The NiMo/Nb-SBA-15 catalyst led to formation of slightly higher amount of DH than the other two Nb-SBA-15 based catalysts.

The catalyst most selective to DH appeared to be the NiMo/Nb-HMS catalyst pointing out on insufficient promotional effect of Ni. Its impregnation with TGA resulted, on one hand, in the improved promotion of Mo by Ni, which was manifested by lower selectivity to dihydrobenzothiophene (DH). On the other hand, the TGA impregnation of NiMo-catalysts in oxide form led to three-dimensional Mo species (Fig. 6), which resulted in lower HDS activity.

In these respects, the present study on C=C hydrogenation to C–S hydrogenolysis (HYD/HYG) selectivity of the 1-benzotiophene HDS, gave results similar to those in the literature [58–63] with dibenzothiophene as a model compound, where an increase in total HDS activity by promotion was accompanied by much greater increase in the direct desulfurization (DDS) reactivity pathway than the HYD reactivity pathway.

The insight into correlation of morphological aspects of promoted Mo catalysts and DDS/HYD selectivity could be found elsewhere in the literature. For example, in the study with high resolution transmission electron microscopy, the DDS pathway was found as the main pathway during HDS of dibenzothiophene [62,63] or benzothiophene [64]. In contrast, the HYD pathway seemed to be essential in the case of the resistant 4,6-dimethyldibenzothiophene HDS [58,60,61].

4. Conclusions

The catalytic performance of the studied NiMo HDS catalysts prepared over Nb modified mesoporous supports is sensitive to the porous structure of the supports and to the way of treatment of the supports/catalysts with thioglycolic acid. The Nb-HMS supported NiMo catalyst shows a slightly higher thiophene and 1-benzothiophene HDS activity in comparison to that of the catalyst supported on Nb-SBA-15.

Impregnation of the calcined NiMo catalysts with a chelating thioglycolic acid changes the HDS performance: activity of the NiMo catalysts supported on Nb-SBA-15 is increased about two times, while that of the catalyst supported on Nb-HMS is significantly decreased. A simultaneous deposition of TGA, Ni and Mo precursors on both supports substantially increases the catalytic activity in the HDS of 1-benzothiophene. Moreover, the Nb-SBA-15 supported NiMoTGA catalyst showed the highest activities in both HDS reactions. Furthermore, this catalyst showed higher activity in HDS of 1-benzothiophene than the reference industrial $NiMo/Al_2O_3$ catalyst.

The larger pore dimensions in Nb-SBA-15 in addition to a higher Nb surface concentration provide more convenient conditions for better dispersion and promotion of the active components on the support, leading as a consequence to a higher HDS catalytic activity.

Acknowledgements

Scientific Cooperation Funds of Bulgarian and Czech Academy are gratefully acknowledged. L.K. appreciates and acknowledges the Czech Science Foundation (project no. P106/11/0902) and Albemarle (The Netherlands) company for financial support and providing of the reference catalyst, respectively.

Appendix A. Supplementary data

Supplementary data associated with this article can be found, in the online version, at http://dx.doi.org/10.1016/j.apcata.2016.04.008.

References

[1] C. Song, Catal. Today 86 (2003) 211–263.
[2] H. Topsøe, B.S. Clausen, F.E. Massoth, Hydrotreating Catalysis, Springer, Berlin, 1996.
[3] A. Infantes-Molina, A. Romero-Perez, V. Sanchez-Gonzalez, B. Pawelec, J.L.G. Fierro, A. Jimenez-Lopez, E. Rodríguez-Castellon, ACS 1 (2011) 175–186.
[4] D. Solís-Casados, J. Escobar, I. García Orozco, T. Klimova, Ind. Eng. Chem. Res. 50 (2011) 2755–2761.
[5] Ch. Geantet, J. Alfonso, M. Breysse, N. Allali, M. Danot, Catal. Today 28 (1996) 23–30.
[6] N. Allali, E. Prouzet, A. Michalowicz, V. Gaborir, A. Nadiri, M. Danot, Appl. Catal. A: Gen. 159 (1997) 333–354.
[7] N. Allali, A. Leblanc, M. Danot, Ch. Geantet, M. Vrinat, M. Breysse, Catal. Today 27 (1996) 137–144.
[8] P. Schacht, S. Ramirez, J. Ancheyta, Energy Fuels 23 (2009) 4860–4865.
[9] T. Klimova, J. Reyes, O. Gutiérrez, L. Lizama, Appl. Catal. A: Gen. 335 (2008) 159–171.
[10] T.A. Zepeda, A. Infantes-Molina, J.N. Díaz de León, S. Fuentes, G. Alonso-Núnez, G. Torres-Otanez, B. Pawelec, Appl. Catal. A: Gen. 484 (2014) 108–121.
[11] F. Hoffmann, M. Cornelius, J. Morell, M. Fröba, J. Nanosci, Nanotechnology 6 (2006) 265–288.
[12] A.C. Faro Jr., A.C.B. dos Santos, Catal. Today 118 (2006) 402–409.
[13] E.J.M. Hensen, Y. van der Meer, J.A.R. van Veen, J.W. Niemantsverdriet, Appl. Catal. A: Gen. 322 (2007) 16–32.
[14] X. Tao, Y. Zhou, Q. Wei, G. Yu, Q. Cui, J. Liu, T. Liu, Fuel Proc. Technol. 118 (2014) 200–207.
[15] G. Yu, Y. Zhou, Q. Wei, X. Tao, Q. Cui, Catal. Commun. 23 (2012) 48–53.
[16] H. Li, M. Li, Y. Chu, F. Liu, H. Nie, Appl. Catal. A: Gen. 403 (2011) 75–82.
[17] C.E. Santolalla-Vargas, V.A. Suárez Toriello, J.A. de los Reyes, D.K. Cromwell, B. Pawelec, J.L.G. Fierro, Mater. Chem. Phys. 166 (2015) 105–115.
[18] J.C. Mogica-Betancourt, A. Lopez-Benitez, J.R. Montiel-Lopez, L. Massin, M. Aouine, M. Vrinat, G. Berhault, A. Guevara-Lara, J. Catal. 313 (2014) 9–23.
[19] G. Wan, A. Duan, Y. Zhang, Z. Zhao, G. Jiang, D. Zhang, Z. Gao, J. Liu, K.H. Chung, Energy Fuels 23 (2009) 3846–3852.
[20] A. Duan, Z. Gao, Q. Huo, C. Wang, D. Zhang, M. Jin, G. Jiang, Z. Zhao, H. Pan, K. Chung, Energy Fuels 24 (2010) 796–803.
[21] M.J. Vissenberg, Y. van der Meer, E.J.M. Hensen, V.H.J. de Beer, A.M. van der Kraan, R.A. van Santen, J.A.R. van Veen, J. Catal. 198 (2001) 151–163.
[22] K. Soni, P.E. Boahene, K. Chandra Mouli, A.K. Dalai, J. Adjaye, Appl. Catal. A: Gen. 398 (2011) 27–36.
[23] L.Y. Lizama, T.E. Klimova, J. Mater. Sci. 44 (2009) 6617–6628.
[24] R. Palcheva, L. Dimitrov, G. Tyuliev, A. Spojakina, K. Jiratova, Appl. Surf. Sci. 265 (2013) 309–316.
[25] R. Palcheva, A. Spojakina, G. Tyuliev, K. Jiratova, L. Petrov, Kinet. Catal. 48 (2007) 847–852.
[26] R. Palcheva, A. Spojakina, L. Dimitrov, K. Jiratova, Micropor. Mesopor. Mater. 122 (2009) 128–134.
[27] B. Pawelec, R. Mariscal, J.L.G. Fierro, A. Greenwood, P.T. Vasudevan, Appl. Catal. A: Gen. 206 (2001) 295–307.
[28] M. Sun, D. Nicosia, R. Prins, Catal. Today 86 (2003) 173–189.
[29] J.A.R. van Veen, E. Gerkema, A.M. van der Kraan, A. Knoester, J. Chem. Soc. Chem. Commun. (1987) 1684–1686.
[30] Y. Ohta, T. Shimizu, T. Honna, M. Yamada, Stud. Surf. Sci. Catal. 127 (1999) 161–168.
[31] T. Shimizu, K. Hiroshima, T. Honna, T. Mochizuki, M. Yamada, Catal. Today 45 (1998) 271–276.
[32] K. Inamura, K. Uchikawa, S. Matsuda, Y. Akai, Appl. Surf. Sci. 121/122 (1997) 468–475.
[33] L. Medici, R. Prins, J. Catal. 163 (1996) 38–49.
[34] R. Cattaneo, T. Shido, R. Prins, J. Catal. 185 (1999) 199–212.
[35] L. Coulier, V.H.J. de Beer, J.A.R. van Veen, J.W. Niemantsverdriet, J. Catal. 197 (2001) 26–33.
[36] T. Kubota, N. Hosomi, K.K. Bando, T. Matsui, Y. Okamoto, Phys. Chem. Chem. Phys. 5 (2003) 4510–4515.
[37] P. Mazoyer, C. Geantet, F. Diehl, S. Loridant, M. Lacroix, Catal. Today 130 (2008) 75–79.
[38] R. Iwamoto, N. Kagami, A. Iino, J. Jpn. Petrol. Inst. 48 (2005) 237–242.
[39] N. Frizi, P. Blanchard, E. Payen, P. Baranek, M. Rebeilleau, C. Dupuy, J.P. Dath, Catal. Today 130 (2008) 272–282.
[40] V. Costa, K. Marchand, M. Digne, C. Geantet, Catal. Today 130 (2008) 69–74.
[41] P. Schneider, Appl. Catal. A: Gen. 129 (1995) 157–165.
[42] J.H. Scofield, J. Electron Spectros, Relat. Phenom. 8 (1976) 129–137.
[43] L. Kaluža, D. Gulková, Z. Vít, M. Zdražil, Fuel 112 (2013) 272–276.
[44] S.J. Greg, K.S.W. Sing, Adsorption, Surface Area and Porosity, second, Academic Press, New York, 1982.
[45] D.Y. Zhao, J.L. Feng, Q.S. Huo, N. Melosh, G.H. Fredrickson, B.F. Chmelka, G.D. Stucky, Science 279 (1998) 548–552.
[46] M. Nishimura, K. Asakura, P. Iwasawa, J. Chem. Soc. Chem Commun. 22 (1986) 1660–1661.
[47] O.Y. Gutierrez, T. Klimova, J. Catal. 281 (2011) 50–62.
[48] J. Abart, E. Delgado, G. Ertl, H. Jeziorowski, H. Knozinger, N. Thiele, X.Zh. Wang, E. Taglauer, Appl. Catal. 2 (1982) 155–176.
[49] A. Cervilla, A. Llopis, J.A. Ramırez, A. Domenech, P. Palanca, M.T. Pilcher, C.A. Guilardi, A. Orlandini, J. Chem. Soc. Dalton Trans. (1994) 175–183.
[50] W. Yang, C. Lu, S. Lu, H. Zhuang, Helv. Chim. Acta 85 (2002) 2417–2429.
[51] J.F. Martin, J.T. Spence, J. Phys. Chem. 74 (1970) 3589–3596.
[52] P.M. Rao, A. Wolfson, S. Kababya, S. Vega, M.V. Landau, J. Catal. 232 (2005) 210–225.
[53] A. Bordoloi, S.B. Halligudi, J. Catal. 257 (2008) 283–290.
[54] H. Jeziorowksi, H. Knozinger, J. Phys. Chem. 83 (1979) 1166–1173.
[55] C. Brookes, P.P. Wells, G. Cibin, N. Dimitratos, W. Jones, D.J. Morgan, M. Bowker, ACS Catal. 4 (2014) 243–250.
[56] Y.G. Wang, G. Xiong, X. Liu, X.C. Yu, L.P. Liu, J.Y. Wang, Z.C. Feng, C. Li, J. Phys.Chem. C. 112 (2008) 17265–17271.
[57] L. Cedeño, D. Hernandez, T. Klimova, J. Ramirez, Appl. Catal. A: Gen. 241 (2003) 39–50.
[58] D. Pérez-Martínez, S.A. Giraldo, A. Centeno, Appl. Catal. A: Gen. 315 (2006) 35–43.
[59] M. Egorova, R. Prins, J. Catal. 225 (2004) 417–427.
[60] F. Bataille, J.L. Lemberton, P. Michaud, G. Pérot, M. Vrinat, M. Lemaire, E. Schulz, M. Breysse, S. Kasztelan, J. Catal. 191 (2000) 409–422.
[61] H. Farag, D.D. Whitehurst, I. Mochida, Ind. End. Chem. Res. 37 (1998) 3533–3539.
[62] D. Gao, A. Duan, X. Zhang, Z. Zhao, E. Hong, J. Li, H. Wang, Appl. Catal. B 165 (2015) 269–284.
[63] L. Yue, G. Li, F. Zhang, L. Chen, X. Li, X. Huang, Appl. Catal. A: Gen. 512 (2016) 85–92.
[64] A. Duan, T. Li, Z. Zhao, B. Liu, X. Zhou, G. Jiang, J. Liu, Y. Wei, H. Pan, Appl. Catal. B 165 (2015) 763–773.